Engineering and Applied Sciences
2026, Vol. 11, No. 5, pp. 164–178
https://doi.org/10.11648/j.eas.20261105.12

Research Article

Effect of CIGS Absorber Thickness on the Performance of In_2S_3-Buffered Thin-Film Solar Cells: Role of the MgF_2 Antireflection Coating

Papa Lat Tabara Sow[1], Cheick Tidiane Goudiaby[2], Alioune Ngom[2], Jacques Joachim Faye[2], Ahmed Mohamed-Yahya[3], Mamadou Lamine Samb[2,*]

[1]Department of Physics, Alioune Diop University, Bambey, Senegal

[2]Department of Physics and Chemistry & UFR Sciences and Technologies, Iba Der Thiam University, Thies, Senegal

[3]Applied Research Unit for Renewable Energies, University of Nouakchott, Nouakchott, Mauritania

Abstract

This work numerically investigates, using the Silvaco ATLAS simulator, a thin-film solar cell based on a Cu(In,Ga)Se_2 (CIGS) absorber combined with a non-toxic In_2S_3 buffer layer replacing conventional CdS, building on an earlier doping-optimization study that identified $N_A = 3\times10^{16}$ cm^{-3} as optimal for both configurations investigated (with and without a MgF_2 antireflection coating). At this doping level, two otherwise identical structures, one with MgF_2 and one without, are compared to isolate the effect of CIGS absorber thickness (0.5 to 4 µm) on J_{sc}, V_{oc}, FF and η. Efficiency increases monotonically with thickness, reaching 24.7% with MgF_2 and 21.93% without at 4 µm, a nearly constant relative gain of about 12.6% attributable almost entirely to the increase in short-circuit current. The analysis also tracks the effective series (R_s) and shunt (R_{sh}) resistances extracted from the simulated J–V curves to clarify the mechanism behind the improvement of the fill factor with thickness. The decrease in Rs and increase in R_{sh} are consistent with reduced electrical losses in thicker absorbers, though these values are read as effective electrical descriptors rather than direct proof of a microstructural change, since no grain-boundary or defect-density model was varied with thickness. A marginal-gain analysis of the full thickness interval, combined with a relative active-material-use analysis, identifies 2–3 µm with MgF_2 as the best trade-off between performance and material use. A particularly compact illustration is that a 1 µm CIGS cell with MgF_2 (η = 22.17%) already outperforms a 4 µm cell without MgF_2 (η = 21.93%), using only a quarter of the absorber volume, showing that improved front-surface optical management can compensate for a substantial reduction in absorber thickness.

Keywords

CIGS, In_2S_3, MgF_2 Antireflection Coating, Absorber Thickness, Series Resistance Rs, Shunt Resistance Rsh, Silvaco ATLAS, Thin-Film Solar Cells

*Correspondence: Mamadou Lamine Samb (mlsamb@univ-thies.sn)

Received: 3 September 2026; **Accepted:** 11 September 2026; **Published:** 27 September 2026

1. Introduction

Solar cells convert sunlight directly into electrical energy [1]. Among second-generation technologies, thin-film solar cells have attracted growing interest owing to their lower fabrication cost and reduced raw-material consumption compared with crystalline silicon. Non-silicon semiconductors such as cadmium telluride (CdTe) and copper indium gallium diselenide Cu(In,Ga)Se_2 (CIGS) are the object of sustained worldwide research aimed at reconciling low cost with high conversion efficiency [2-4].

CIGS-based solar cells offer several advantages over silicon cells: high efficiency, good stability under prolonged illumination, and a high absorption coefficient characteristic of a direct-gap semiconductor. CIGS is a p-type semiconductor whose bandgap is tunable between about 1.0 and 1.7 eV depending on the Ga/(In + Ga) ratio [4], allowing satisfactory efficiency with an absorber thickness of only 1–2 μm, against several tens of micrometers for crystalline silicon [1, 5].

Advances in research and development have driven a continuous rise in the record efficiency of laboratory CIGS cells: 19.9% in 2008 [6], above 20% in 2011 [7], 22.6% in 2016 through heavy-alkali post-deposition treatment [8], and 23.35% in 2019 for a cadmium-free configuration [9]. These gains still rely heavily on a high indium and gallium content, two costly elements of limited availability. Reducing the absorber thickness can lower material consumption, but experimentally it may also be accompanied by reduced long-wavelength absorption and, depending on the deposition process, changes in crystalline quality that can penalize conversion efficiency. Several strategies have been explored to compensate for this loss in thinned absorbers, for example adding a second low-cost absorbing layer [10], which underlines that absorber thickness remains, despite these alternative approaches, a key parameter requiring careful optimization.

The present study follows this logic. In addition to absorber thickness, the buffer layer forming the heterojunction with CIGS plays a decisive role: cadmium sulfide (CdS), traditionally used, provides good band alignment but is toxic and has a relatively narrow gap (~2.42 eV) that limits its large-scale industrial deployment [3]. Indium sulfide In_2S_3 is a widely studied non-toxic alternative whose wider gap and good optical transparency have enabled certified efficiencies above 16% [11]. On the front side, front-surface reflection losses can further be reduced by depositing an antireflection coating such as magnesium fluoride (MgF_2). MgF_2 was selected here not as a novel antireflection material per se, but because its low refractive index, high transparency over the relevant solar spectral range, and established use in CIGS front stacks make it a suitable single-layer reference coating. Compared with higher-index coatings such as SiN_x, MgF_2 provides a favorable refractive-index transition between air and the transparent conductive oxide. The novelty of the present work therefore lies in quantifying how this optical benefit interacts with CIGS absorber thinning in an In_2S_3-buffered architecture, including the resulting performance/material-use trade-off.

The objective of this work is therefore to quantify, through Silvaco ATLAS numerical simulation, the influence of CIGS absorber thickness (0.5 to 4 μm) on the short-circuit current density (Jsc), open-circuit voltage (Voc), fill factor (FF), and conversion efficiency (η) of an In_2S_3-buffered solar cell, and to isolate the specific contribution of the MgF_2 antireflection coating by comparing two otherwise identical structures with and without this layer. The analysis is enriched by tracking the evolution of the effective series (Rs) and shunt (Rsh) resistances in order to clarify their association with the improvement of the fill factor with thickness.

2. Simulation Methodology

The simulations were performed with the SILVACO ATLAS software [12], a semiconductor device simulator based on the self-consistent two- and three-dimensional solution of the fundamental carrier-transport equations, including Poisson's equation, the continuity equations, and the drift-diffusion transport equations at every mesh node [5].

Poisson's equation

Poisson's equation relates the electrostatic potential to the space-charge density within the device:

$$\mathrm{div}(\varepsilon\nabla\psi) = -\rho \tag{1}$$

where ψ is the electrostatic potential, ε the local permittivity and ρ the local space-charge density. The space-charge density is the sum of the contributions of all mobile and fixed charges, including electrons, holes and ionized impurities. Equation (1) then becomes:

$$\mathrm{div}(\nabla\psi) = \Delta\psi = -\frac{q}{\varepsilon}[p - n + N_D^+ - N_A^-] \tag{2}$$

where n and p are the electron and hole densities, and N_D^+ and N_A^- the ionized donor and acceptor densities.

Continuity equations

The continuity equations describe the time evolution of carrier concentrations as a function of current densities and generation/recombination rates:

$$\frac{\partial n}{\partial t} = \frac{1}{q}\mathrm{div}\overrightarrow{J_n} + G_n - R_n \tag{3}$$

$$\frac{\partial p}{\partial t} = -\frac{1}{q}\mathrm{div}\overrightarrow{J_p} + G_p - R_p \tag{4}$$

where n and p are the electron and hole concentrations, $\vec{J}_n$ and $\vec{J}_p$ the electron and hole current densities, G_n and G_p the generation rates, R_n and R_p the recombination rates, including Shockley-Read-Hall recombination [13], and q the elementary charge.

Transport equations

Carrier transport is described by the drift-diffusion model. The electron and hole current densities are given respectively by:

$$\vec{J}_n = qn\mu_n\vec{E}_n + qD_n\nabla n \quad (5)$$

$$\vec{J}_p = qp\mu_p\vec{E}_p - qD_p\nabla p \quad (6)$$

where μ_n and μ_p are the electron and hole mobilities, and $\vec{E}_n$, $\vec{E}_p$ the effective electric fields defined by:

$$\vec{E}_n = -\nabla\left(\psi + \frac{K_BT}{q}\ln(n_i)\right) \quad (7)$$

$$\vec{E}_p = -\nabla\left(\psi - \frac{K_BT}{q}\ln(n_i)\right) \quad (8)$$

D_n and D_p are the electron and hole diffusivities, related to the mobilities by the Einstein relation:

$$D_{n,p} = \frac{\mu_{n,p}K_BT}{q} \quad (9)$$

2.1. Cell Structure

Two otherwise identical structures were simulated to isolate the effect of the antireflection coating: one including the MgF_2 layer, the other without, with only the CIGS absorber thickness swept from 0.5 to 4 µm. Figure 1 shows a cross-section of the structure as generated under Silvaco ATLAS (Tonyplot module) for the MgF_2 configuration.

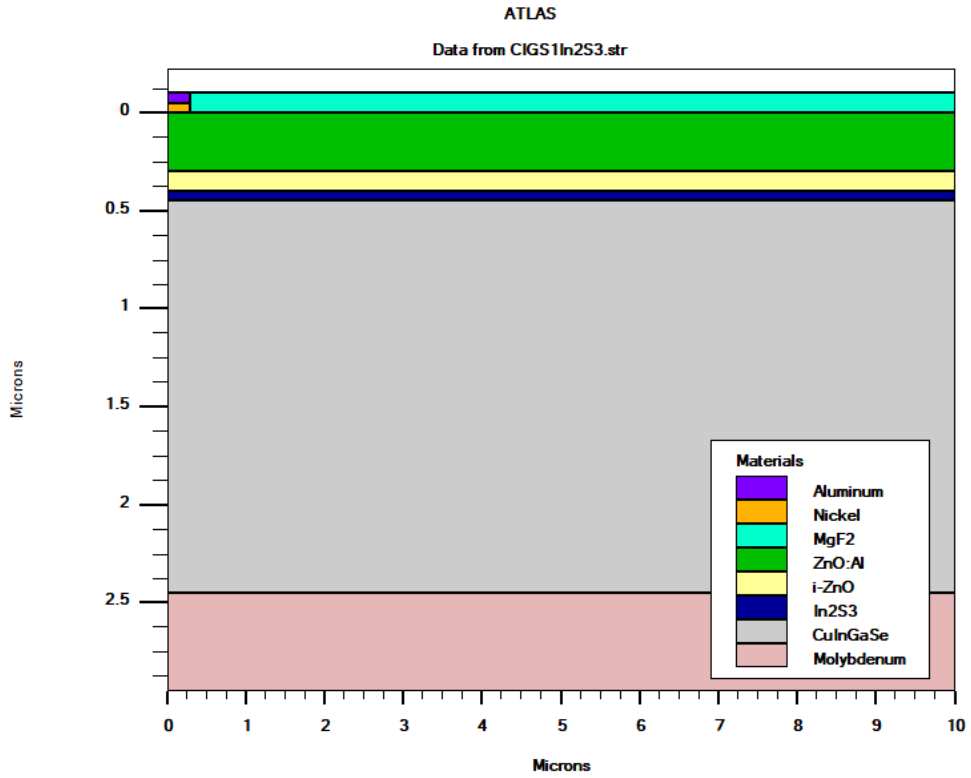

Figure 1. *Layer stack of the CIGS/In_2S_3 structure simulated under Silvaco ATLAS, including the MgF_2 antireflection coating.*

The layer stack, from the front side to the back contact, is summarized in Table 1 below.

Table 1. *Layer stack and role of each layer in the CIGS/In_2S_3/MgF_2 structure simulated under Silvaco ATLAS.*

Layer	Role
Aluminum / Nickel	Front metal contact (grid)
MgF_2	Antireflection coating
ZnO:Al	Transparent conductive oxide (TCO)

Layer	Role
i-ZnO	Intrinsic window layer
In_2S_3	Buffer layer (heterojunction with CIGS)
CIGS ($Cu(In,Ga)Se_2$)	Main absorber
Molybdenum (Mo)	Back contact

2.2. Band Diagram at the In_2S_3 Interface

Figure 2 shows the band diagram extracted along a cross-section through the i-ZnO, In_2S_3 and CIGS layers at equilibrium. A conduction-band discontinuity (spike) is observed at the In_2S_3/CIGS interface, with the conduction band rising by about +0.3 eV on the In_2S_3 side to a maximum close to 1.1 eV before stabilizing on the CIGS side. The valence band shows a much more pronounced offset, dropping to about −3 eV on the In_2S_3 side before rising sharply near the interface to reach a level close to 0 eV on the CIGS side. A moderate conduction-band spike such as the one observed here is generally considered favorable to electron collection as long as it remains within the approximately 0–0.4 eV range [14]; a substantially larger spike may act as a transport barrier. The large valence-band offset provides strong hole confinement on the CIGS side; however, its net impact on interface recombination also depends on the density and energetic distribution of interface states and cannot be inferred from band alignment alone.

This band diagram, obtained for the reference structure, is assumed to remain qualitatively representative over the entire CIGS thickness range studied, since absorber thickness does not directly affect band alignment at the In_2S_3/CIGS interface. MgF_2, a purely optical and electrically neutral layer owing to its refractive index intermediate between air and the TCO, does not enter this band diagram; the structure without MgF_2 therefore shows a rigorously identical band diagram and is not reproduced separately.

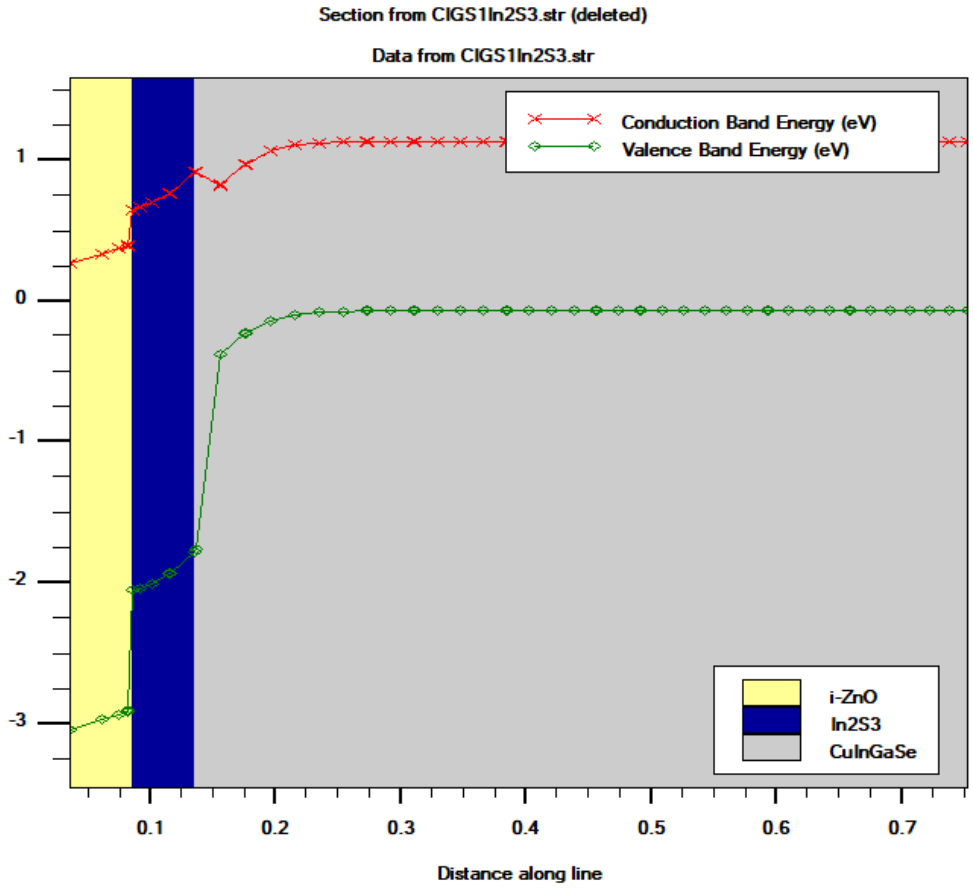

Figure 2. *Conduction- and valence-band diagram near the In_2S_3/CIGS heterojunction.*

2.3. Simulation Input Parameters

Table 2 gathers the physical and electronic parameters of the ZnO:Al, i-ZnO, In_2S_3 and CIGS layers used for this type of structure at the optimal doping level $N_A = 3\times10^{16}$ cm^{-3}.

The parameters retained for the ZnO:Al window and i-ZnO intrinsic layers correspond to standard values commonly adopted in ATLAS/SCAPS simulation studies of CIGS cells [15, 16]; those of In_2S_3 (optical gap, effective density of states and donor density) are taken from a dedicated optimization study of this buffer layer [17]; the interface defect density D_{it} is taken from the analysis of the window/absorber conduction-band offset [14]; the CIGS parameters (gap, electron affinity, mobilities, lifetimes) correspond to the reference values from the chapter devoted to Cu(In,Ga)Se_2 in the Handbook of Photovoltaic Science and Engineering [4] and are consistent with those adopted in an earlier TCAD study of this same ZnO:Al/i-ZnO/In_2S_3/CIGS structure [18]. All of these material parameters were held fixed throughout the thickness sweep, so that only the CIGS absorber thickness (the parameter of interest, explicitly listed in Table 2 as 0.5, 1, 2, 3 and 4 µm) differs between simulation runs, isolating its effect from any other electronic parameter.

The MgF_2 layer, being purely optical, does not appear in this table of electronic parameters; its only properties relevant to the simulation are its thickness (105 nm, fixed throughout the thickness sweep; see Section 3.5) and refractive index ($n \approx 1.38$), which enter the optical calculation of the carrier generation profile rather than the electrical solution of the device.

Table 2. *Physical parameters used in the ATLAS simulation for the ZnO:Al, i-ZnO, In_2S_3 and CIGS layers.*

Parameters	ZnO:Al	i-ZnO	In_2S_3	CIGS
Optical gap Eg (eV) at 300 K	3.3	3.3	2.7	1.2
Electron affinity χ (eV)	4.45	4.45	4.2	4.5
Relative permittivity ε_r	9	9	13.5	13.6
Thickness d (µm)	0.3	0.1	0.05	0.5, 1, 2, 3 and 4
Effective density of states N_C (cm^{-3}) at 300 K	2.2×10^{18}	2.2×10^{18}	2×10^{19}	2.2×10^{18}
Effective density of states N_V (cm^{-3}) at 300 K	1.8×10^{19}	1.8×10^{19}	2×10^{17}	1.8×10^{19}
Donor concentration N_D (cm^{-3})	10^{20}	10^{14}	10^{17}	—
Acceptor concentration N_A (cm^{-3})	—	—	—	3×10^{16}
Electron mobility µn ($cm^2 \cdot V^{-1} \cdot s^{-1}$)	100	100	50	100
Hole mobility µp ($cm^2 \cdot V^{-1} \cdot s^{-1}$)	25	25	15	25
Electron lifetime τ_n (s)	10^{-10}	10^{-10}	10^{-9}	10^{-7}
Hole lifetime τ_p (s)	10^{-10}	10^{-10}	10^{-9}	10^{-7}
Interface defect density D_{it} ($cm^{-2}.eV^{-1}$)	—	—	8×10^{11}	—

2.4. Photovoltaic Output Parameters

Current-voltage (J-V) characteristics were simulated under standard AM1.5G illumination (100 mW/cm^2) at room temperature (300 K). The extracted photovoltaic parameters include:

Short-circuit current density (J_{SC}): the current generated per unit area when V = 0. It results mainly from the transport of minority carriers generated by the absorption of incident photons, and can be expressed as:

$$J_{SC} = q\int_0^{\lambda_g} E(\lambda)\frac{\lambda}{hc}\mathrm{EQE}(\lambda)d\lambda \quad (10)$$

where J_{SC} is the short-circuit current density ($A\cdot m^{-2}$), λ_g the wavelength corresponding to the optical gap energy (m), λ the wavelength of the incident radiation (m), h Planck's constant (J s), c the speed of light in vacuum ($m\cdot s^{-1}$), EQE the external quantum efficiency and q the elementary charge.

Open-circuit voltage (V_{OC}): the voltage across the cell when J = 0, defined by:

$$V_{OC} = \frac{nKT}{q}\ln\left(\frac{J_{SC}}{J_0}+1\right) \quad (11)$$

where n is the ideality factor, K Boltzmann's constant, T the absolute temperature, q the elementary charge, J_{SC} the

short-circuit current density (A cm^{-2}) and J_0 the saturation current density (A cm^{-2}).

Fill factor (FF): also known as the fill factor, expresses the electrical quality of the cell as the ratio of the actual maximum delivered power to the ideal maximum power:

$$FF = \frac{Jm \times Vm}{Jsc \times Voc} \quad (12)$$

where FF is the fill factor (%), J_m the current density at the maximum-power point (A cm^{-2}), V_m the corresponding voltage (V), J_{SC} the short-circuit current density and V_{OC} the open-circuit voltage.

Power conversion efficiency (η): the ratio of the maximum electrical power to the incident optical power, used to assess the overall efficiency of the solar cell:

$$\eta = \frac{P_m}{P_{in}} = FF \cdot \frac{Jsc \times Voc}{P_{in}} \quad (13)$$

where P_m is the maximum delivered power (W), P_{in} the incident power (W), FF the fill factor (%) and η the power conversion efficiency (%).

In addition to these four macroscopic quantities, the J-V characteristic allows two parasitic resistances to be extracted; together they govern the shape of the curve around the maximum-power point. In the single-diode electrical model, the series resistance R_s is extracted from the local slope −(dV/dJ) of the J-V characteristic near V_{oc}, and the shunt resistance R_{sh} from the slope near J_{sc} [19]. As detailed in Section 3.4 below, these two quantities should be understood as *effective* resistances describing the simulated J-V curve, rather than as independently imposed physical parameters of the device: no grain-boundary, defect-density or microstructural model was varied together with thickness in the present simulations. Nonetheless, jointly acting to reduce the power actually extracted from the cell, they translate directly into a rounding of the knee of the J-V characteristic and hence into a degraded fill factor. This selective sensitivity to the fill factor makes R_s and R_{sh} diagnostic indicators complementary to the four usual photovoltaic parameters. The optical-generation profile calculation further incorporates the complex refractive indices of the different layers, including those of CIGS and MgF_2 [20].

2.5. Model Consistency

Before examining the effect of thickness, it is useful to note that the present simulation setup reproduces, as a limiting case, the result of the earlier doping-optimization study on which it builds [18]. That precursor study, using the same layer stack and the same optimal doping level $N_A = 3\times10^{16}$ cm^{-3} at a fixed absorber thickness of 2 µm, reported efficiencies of 23.65% (with MgF_2) and 20.99% (without MgF_2). The 2 µm point of the present thickness sweep reproduces these values exactly (Figure 6), since both studies share the same input-parameter set and simulation environment. While this is an internal consistency check rather than an independent experimental validation, it confirms that no parameter drift was introduced between the two studies and that the present sweep is a genuine extension, rather than a re-derivation, of the earlier doping-optimization result. More broadly, the efficiency range obtained here (18.1%–24.7% depending on configuration and thickness) is consistent with the range reported in the wider SCAPS/ATLAS literature on In_2S_3-buffered CIGS cells, which spans from the certified 16% obtained experimentally on early In_2S_3 buffer devices [11] to the 20%–26% range reported by several numerical optimization studies on related architectures [16, 17].

3. Results and Discussion

3.1. J-V Characteristics Over the Studied Thickness Range

Figure 3 compares the complete simulated J–V characteristics obtained for the five CIGS thicknesses in the presence and absence of the MgF_2 coating. Rather than discussing the individual photovoltaic parameters at this stage, which are analyzed quantitatively in the following sections, Figure 3 provides an overall view of how absorber thickness modifies the current plateau and the maximum-power region of the device. For each thickness, the MgF_2-coated configuration displays a higher photocurrent while the two configurations approach similar V_{oc} values near the knee of the characteristic. The maximum delivered power reaches about 24.7 mW/cm^2 with MgF_2 and 21.9 mW/cm^2 without MgF_2 at 4 µm, consistent with the efficiencies reported in Figure 6 under AM1.5G illumination of 100 mW/cm^2.

Figure 3a-b show, for each configuration, the complete families of J(V) curves at the five studied thicknesses (0.5 to 4 µm), illustrating the progressive narrowing of the curves. The resulting P(V) characteristics (P = J·V) are not reproduced, but their derived quantities (P_{max}, FF, η) appear in Figure 6. The numerical values discussed in the text refer, unless otherwise stated, to the extreme 4 µm curve for each configuration; the detailed analysis of the full interval, essential to establishing a performance/material-use trade-off, is developed in Sections 3.2 to 3.7 from Figures 4 to 7 and Tables 3 to 6.

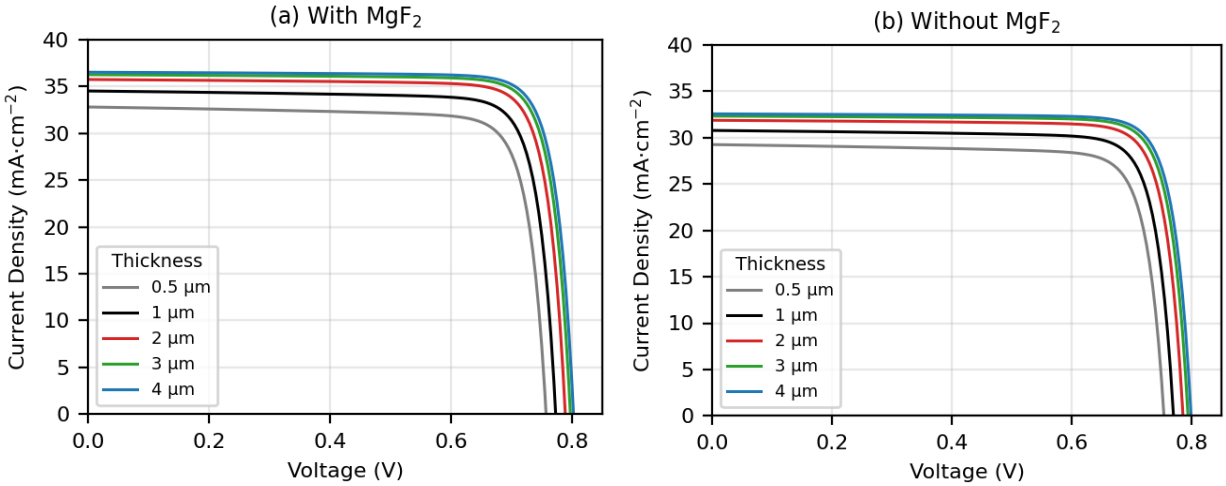

Figure 3. *Current-voltage characteristic J(V) (a) with MgF_2 antireflection coating and (b) without MgF_2 antireflection coating, for CIGS thicknesses of 0.5, 1, 2, 3 and 4 µm ($N_A = 3\times10^{16}$ cm^{-3}).*

3.2. Effect of Thickness on Short-Circuit Current (Jsc) and Open-Circuit Voltage (Voc)

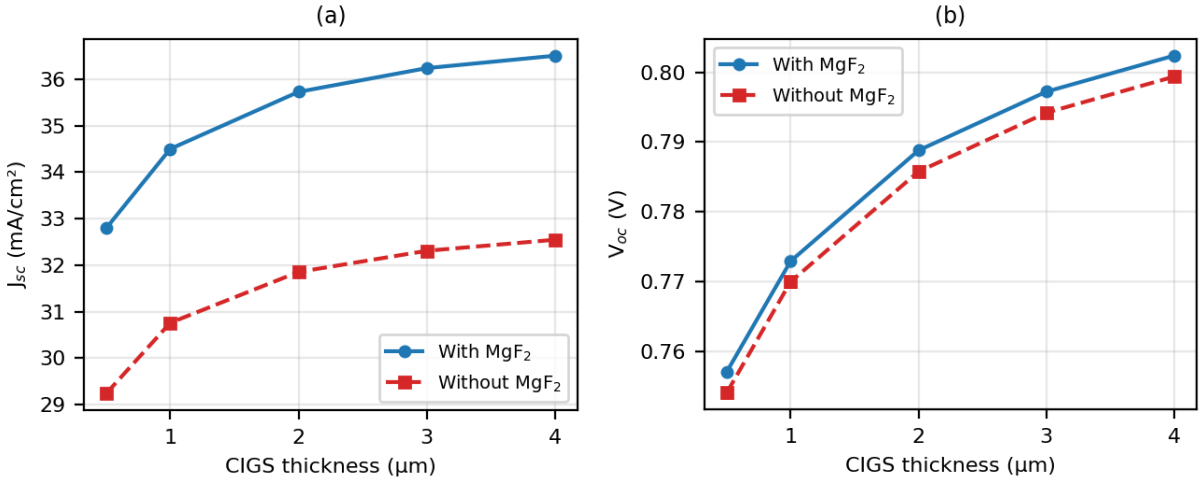

Figure 4. *Evolution of short-circuit current J_{sc} (a) and open-circuit voltage V_{oc} (b) as a function of CIGS absorber thickness, with and without MgF_2 antireflection coating.*

The short-circuit current increases monotonically with CIGS thickness, from 29.2 to 32.5 mA/cm² without MgF_2 (+11.3%) and from 32.8 to 36.5 mA/cm² with MgF_2 (+11.3% as well). This reflects the increased absorption of long-wavelength photons as the volume of active material grows, with progressive saturation beyond 2.5–3 µm once nearly all of the useful spectrum is absorbed [15]. The nearly constant gap of about 3.5–4 mA/cm² between the two curves is attributable to the reduction of front-surface reflection losses provided by MgF_2, independently of thickness.

This behavior can be quantified directly from Figure 4 using a marginal-gain indicator, $S_{Jsc} = \Delta J_{sc}/\Delta d$, expressed in mA $cm^{-2}\cdot\mu m^{-1}$ (Table 3), i.e. the additional short-circuit current gained per additional micrometer of absorber. With MgF_2, S_{Jsc} decreases from 3.42 mA $cm^{-2}\cdot\mu m^{-1}$ between 0.5 and 1 µm to 0.27 mA $cm^{-2}\cdot\mu m^{-1}$ between 3 and 4 µm, a reduction by a factor of about 13 that quantitatively confirms the progressive saturation of J_{sc}. This saturation reflects an optical mechanism intrinsic to CIGS: as a direct-gap semiconductor, its absorption coefficient α rises rapidly above E_g [1, 4, 5], so that nearly all of the useful photons are absorbed within the first micrometer; only photons near the absorption edge ($\lambda_g = hc/E_g \approx 1.03$ µm for $E_g \approx 1.2$ eV) require additional thickness. Following the Beer-Lambert law, $A(d) = 1 - \exp(-\alpha d)$, J_{sc} grows monotonically but asymptotically, so that each additional micrometer captures a progressively smaller fraction of the remaining useful flux, hence the narrowing of the curves beyond 2.5–3 µm, consistent with the literature [4, 15].

Table 3. *Marginal short-circuit current gain $S_{Jsc} = \Delta J_{sc}/\Delta d$, with and without MgF_2.*

Thickness interval (µm)	S_{Jsc} with MgF_2 (mA·cm^{-2}·µm^{-1})	S_{Jsc} without MgF_2 (mA·cm^{-2}·µm^{-1})
0.5–1	3.42	3.05
1–2	1.23	1.09
2–3	0.51	0.46
3–4	0.27	0.24

The saturation of Jsc observed beyond 2.5–3 µm (Table 3) remains, within the studied interval, predominantly optical rather than transport-related: the parameters in Table 2 give, via the Einstein relation, an electron diffusion coefficient $D_n \approx 2.6$ cm^2·s^{-1} and hence an electron diffusion length $L_n = \sqrt{(D_n \tau_n)} \approx 5.1\ \mu m$, larger than the greatest simulated thickness (4 µm). This estimate supports the interpretation that carrier transport is unlikely to be the dominant limitation over the investigated thickness range, which is consistent with the absence of any Jsc roll-off at larger thicknesses [21]. This diffusion-length argument is a consistency check rather than a direct demonstration of complete carrier collection, since actual collection also depends on the internal electric field, the space-charge-region extent, and the spatial distribution of bulk and interface recombination. Beyond the investigated 4 µm range, transport and recombination limitations could become progressively more relevant and would require explicit investigation rather than extrapolation from the present sweep.

The open-circuit voltage, for its part, increases more moderately (6.0% without MgF_2, from 0.754 V to 0.799 V). This moderate increase is consistent with the logarithmic dependence of V_{oc} on the ratio between the photogenerated current and the dark recombination current J_0 [5]. In the present simulations, the increase in J_{sc} contributes directly to this evolution, whereas the comparatively small change in V_{oc} indicates that thickness mainly acts through photogeneration rather than through a major modification of the junction electrostatics; since J_0 was not independently extracted in the present study, no specific thickness dependence of the saturation current is inferred here. The gap between the with- and without-MgF_2 configurations on V_{oc} remains small (2–3 mV), consistent with the purely optical nature of the antireflection coating: MgF_2 acts on the photogenerated current, and its effect on V_{oc} is only indirect, through the logarithmic dependence of V_{oc} on the photocurrent.

3.3. Status of the Series (Rs) and Shunt (Rsh) Resistances

In the present study, the series (R_s) and shunt (R_{sh}) resistances are not introduced as independent parameters imposed on the device, but are extracted from the simulated J-V characteristics from the local slopes near V_{oc} and J_{sc} respectively, for each CIGS thickness. They should accordingly be interpreted as *effective* resistances describing the overall electrical shape of the simulated characteristic. Their evolution with absorber thickness therefore constitutes a diagnostic indicator of changes in the device's electrical behavior, without on its own allowing these variations to be attributed to a specific microstructural change in the CIGS layer, since no such change was independently modeled here.

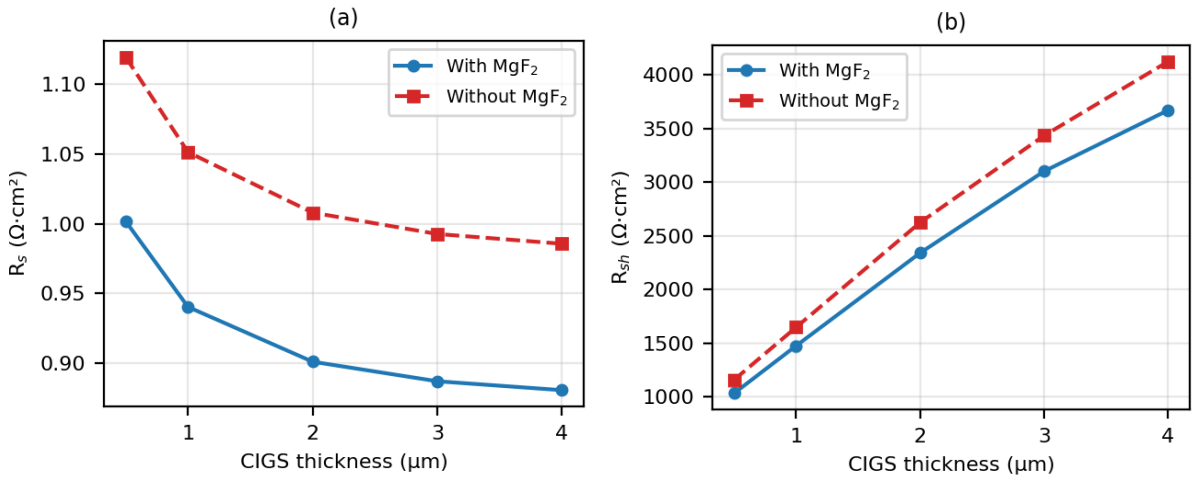

Figure 5. *Evolution of series resistance R_s (a) and shunt resistance R_{sh} (b) as a function of CIGS thickness, with and without MgF_2.*

Two clear trends emerge from Figure 5: R_s decreases monotonically with thickness (about −12% with MgF_2 and −12% without MgF_2 between 0.5 and 4 µm, a nearly identical relative decrease in both configurations), while R_{sh} increases strongly and almost continuously (by a factor of about ×3.5 over the same range). These evolutions are correlated with, rather than direct proof of, the fill-factor improvement observed in the simulations, and are qualitatively consistent with what the experimental literature on thin-film CIGS cells reports: a comparative analysis of published experimental data shows a clear tendency for R_s to increase as the absorber is thinned; for a 230 nm-thick device, a series resistance of about 9 Ω·cm^2 has thus been reported, against 1–2 Ω·cm^2 for absorbers of 1.5–2 µm, with the thickness reduction accompanied experimentally by smaller crystalline grain size and denser grain boundaries, which act as additional potential barriers to carrier transport [21]. A study on the joint influence of CIGS doping and thickness further confirms that insufficient control of these two parameters tends to simultaneously degrade R_s and R_{sh} [22]. The shunt resistance, in turn, is classically associated with the density of parasitic leakage paths (pores, microcracks, local short-circuits crossing the absorber or buffer layer), defects that are more likely to connect the two electrodes as the active layer becomes thinner [23, 24]. A recent parametric study on chalcogenide-based thin-film cells recommends, as a benchmark, keeping R_s below 2 Ω·cm^2 and R_{sh} above 600 Ω·cm^2 to limit efficiency losses [23]. The values obtained here (R_s between 0.88 and 1.12 Ω·cm^2; R_{sh} between about 1000 and 4100 Ω·cm^2) comfortably satisfy this benchmark from 1 µm of thickness onward, consistent with reported experimental trends, though this does not constitute a validation of the extracted values against a specific experimental device.

Over the entire studied thickness range, R_s is systematically lower with MgF_2 than without, and R_{sh} is also lower with MgF_2 at equal thickness, even though MgF_2 is a purely optical dielectric layer that does not a priori modify the physical mechanisms underlying R_s (bulk resistivity, contacts, window layer) or R_{sh} (defects, grain boundaries, short-circuits). A methodological explanation is therefore more plausible: because R_s and R_{sh} are extracted from local slopes of the J(V) characteristic near V_{oc} and J_{sc}, respectively, and MgF_2 substantially changes J_{sc} (Figure 4), the extracted values may partly reflect the sensitivity of the slope-based extraction procedure to the illumination-induced shift of the J–V characteristic rather than a genuine modification of the physical resistive elements. The main qualitative conclusion nonetheless remains robust: increasing CIGS thickness improves the fill factor and is accompanied, in the simulated J–V characteristics, by a decrease in effective R_s and an increase in effective R_{sh}.

3.4. Effect of Thickness on Fill Factor (FF) and Conversion Efficiency (η)

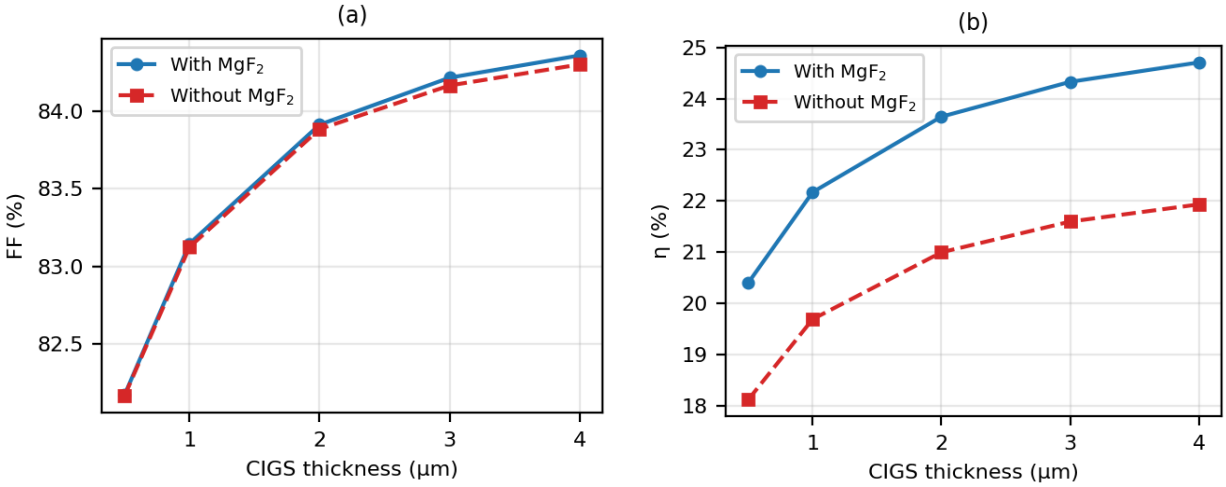

Figure 6. *Evolution of fill factor FF (a) and conversion efficiency η (b) as a function of CIGS absorber thickness, with and without MgF_2 antireflection coating.*

The fill factor increases monotonically with thickness (from 82.2% to 84.3–84.4%), the two curves being nearly superimposed (gap below 0.06 point). Unlike the behavior observed for similar cells as a function of doping, where FF shows an optimum followed by a sharp drop beyond a certain threshold, associated with an Auger recombination regime [25], the evolution with thickness remains monotonic over the whole studied range, with no sign of degradation at 4 µm. This behavior is consistent with the evolution of the parasitic resistances presented in Section 3.3.

The evolution of efficiency η, placed alongside that of the fill factor FF, is shown jointly in Figure 6. Efficiency follows the product J_{sc} ×V_{oc} ×FF: it rises from 18.1% to 21.9% without

MgF_2 and from 20.4% to 24.7% with MgF_2 over the studied range. The relative MgF_2 gain remains nearly constant at about 12.6%, changing only from 12.61% at 0.5 μm to 12.66% at 4 μm. This result indicates that front-surface optical management remains beneficial throughout the absorber-thickness range considered, while the magnitude of the relative gain is largely preserved under the controlled simulation conditions.

3.5. Role of the MgF_2 Antireflection Coating

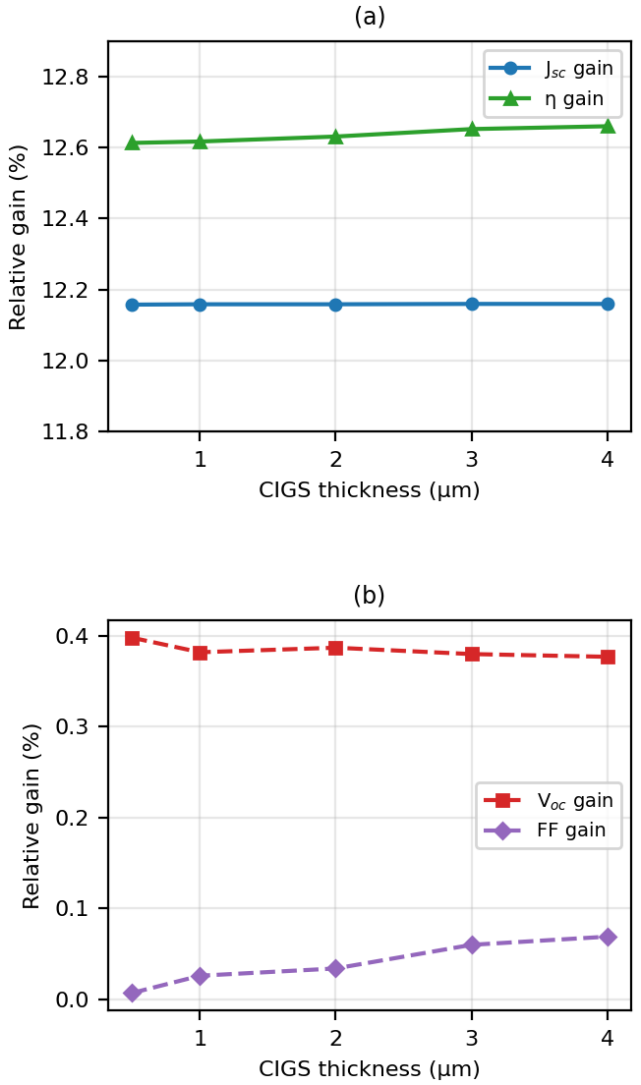

Figure 7. *Relative gain provided by the MgF_2 antireflection coating as a function of CIGS absorber thickness: (a) relative gains in Jsc and conversion efficiency η; (b) relative gains in V_{oc} and fill factor FF.*

The relative gain provided by MgF_2 is nearly invariant across the entire thickness range investigated: the relative J_{sc} improvement remains close to 12.16%, and the efficiency improvement close to 12.6%, whereas V_{oc} and FF change by only about 0.38% and 0.01–0.07%, respectively. This hierarchy is consistent with the predominantly optical role of MgF_2: by reducing front-surface reflection, the coating increases the absorbed photon flux and hence the photogenerated current, while exerting only an indirect influence on V_{oc} and essentially no direct influence on the electrical mechanisms governing FF. The near invariance of the relative gain should not be interpreted as implying that antireflection performance is intrinsically independent of coating thickness. In the present sweep, the MgF_2 thickness and optical constants are deliberately held fixed while only the CIGS absorber thickness is varied; therefore, the coating modifies front-surface optical coupling in essentially the same way for each simulated device. Because the electronic parameter set is also unchanged, the MgF_2-induced photocurrent increase scales approximately with the baseline photocurrent, leading to the observed near-constant relative gain. This behavior is specific to the controlled simulation conditions considered here and should not be generalized to arbitrary MgF_2 thicknesses or to experimentally evolving absorber microstructures.

MgF_2 has a refractive index close to n = 1.38, intermediate between air (n ≈ 1) and transparent-conductive-oxide window layers (ZnO, ITO, n ≈ 1.9–2.0). For a single-layer antireflection coating, the thickness that minimizes reflection through destructive interference follows the quarter-wave condition $d = \lambda/(4n)$ [26, 27]. In the present simulations, the MgF_2 thickness was fixed at 105 nm throughout the CIGS-thickness sweep, corresponding to a target wavelength $\lambda \approx 4nd \approx 580$ nm and falling within the 100–110 nm range reported for CIGS cells [26, 27]. This value was kept unchanged so that the comparison isolates the effect of CIGS absorber thickness. Experimental CIGS studies using MgF_2 front-surface antireflection coatings report the same qualitative mechanism: increased photocurrent and conversion efficiency through reduced reflection. For example, a reported CIGS device fitted with a single MgF_2 layer showed an efficiency increase from 18.99% to 20.52%, corresponding to a relative gain of about 8.1% [28]. The present simulated gain of about 12.6% is somewhat larger, but both results support the same dominant mechanism, namely the enhancement of J_{sc} by improved front-surface optical coupling. Exact numerical agreement is not expected because the present TCAD model keeps material and interface parameters fixed and does not reproduce all experimental optical and microstructural losses. More recent studies further show that double-layer or porous graded-index antireflection designs can provide additional gains compared with a simple single MgF_2 layer [29].

3.6. Absorber-Thickness / Material-Use Trade-off

Efficiency η, resulting from the product $J_{sc} \times V_{oc} \times FF$, inherits the plateauing observed on each of these three quantities, though for distinct reasons. J_{sc} saturates through progressive exhaustion of the absorbable spectrum (Section 3.2). V_{oc} plat-

eaus because its logarithmic dependence on the photogenerated-to-dark-current ratio [4, 19] inherently compresses further gains as J_{sc} itself approaches saturation. FF plateaus because the joint improvement of R_s and R_{sh} (Section 3.3), while favorable, also progressively weakens with thickness. This joint plateauing means that, beyond a certain thickness, increasing the absorber volume, and hence the quantity of indium and gallium consumed [2, 30], yields only a marginal and decreasing efficiency gain, which grounds the 2–3 µm performance/material-use trade-off retained in the conclusion. Because indium and gallium prices fluctuate substantially over time and are not the focus of this study, the analysis below is expressed in terms of relative material volume rather than absolute cost figures.

The preceding sections have established that efficiency increases continuously with CIGS thickness over the whole studied interval (0.5 to 4 µm), with no optimum or degradation. At fixed Ga/(In+Ga) composition and surface area, however, the volume, and hence the mass of In and Ga engaged, grows linearly with thickness. The mere observation of a rising efficiency up to 4 µm is therefore not sufficient on its own. A genuine performance/material-use trade-off requires instead weighing the marginal efficiency gain per micrometer of added thickness against the corresponding increase in material use.

The marginal gain Δη, calculated from Figure 6 and summarized in Table 4, falls sharply as thickness increases: it amounts to about 1.77 points (with MgF_2) and 1.57 points (without MgF_2) between 0.5 and 1 µm, then 1.48/1.31 points between 1 and 2 µm, 0.68/0.60 points between 2 and 3 µm, and only 0.38/0.34 points between 3 and 4 µm, a reduction factor of about 4.5 to 5 between the first and last micrometer added. To make this trend directly comparable across unevenly spaced intervals, Table 4 also reports the normalized marginal gain $S_\eta = \Delta\eta/\Delta d$ in points of efficiency per micrometer. This saturation of the marginal efficiency gain is the direct counterpart of the J_{sc} saturation beyond 2.5–3 µm (Section 3.2), itself consistent with the fact that most of the useful solar spectrum is absorbed by CIGS within the first few micrometers of material [15].

Table 4. *Marginal efficiency gain $\Delta\eta$ and normalized marginal gain $S_\eta = \Delta\eta/\Delta d$ between consecutive thicknesses, with and without MgF_2 (calculated from Figure 6).*

Thickness interval (µm)	Δη with MgF_2 (points)	S_η with MgF_2 (points/µm)	Δη without MgF_2 (points)	S_η without MgF_2 (points/µm)
0.5–1	1.77	3.54	1.57	3.14
1–2	1.48	1.48	1.31	1.31
2–3	0.68	0.68	0.60	0.60
3–4	0.38	0.38	0.34	0.34

In terms of retained efficiency, a 2 µm thickness preserves about 95.7% of the efficiency obtained at 4 µm (23.65%/24.71% with MgF_2; 20.99%/21.93% without MgF_2) while using only 50% of the CIGS volume, hence roughly half the indium and gallium. At 3 µm, this retention rate reaches 98.5% for 75% of the volume used. In other words, reducing thickness from 4 to 2 µm costs only about 4% of relative efficiency for an active-material saving of about 50%. Given that indium and gallium represent important material-cost contributors in CIGS absorbers [30], this represents a materials-reduction lever noticeably more favorable than the performance sacrificed. Table 5 summarizes, for each thickness, the relative CIGS volume engaged and the retained efficiency relative to the maximum obtained at 4 µm.

Table 5. *Relative CIGS volume engaged and retained efficiency (as % of the maximum efficiency at 4 µm), as a function of thickness.*

Thickness (µm)	Relative CIGS volume at 4 µm (%)	Retained η with MgF_2 (% of max.)	Retained η without MgF_2 (% of max.)
0.5	12.5	82.6	82.6
1	25	89.7	89.8
2	50	95.7	95.7

Thickness (µm)	Relative CIGS volume at 4 µm (%)	Retained η with MgF_2 (% of max.)	Retained η without MgF_2 (% of max.)
3	75	98.5	98.5
4	100	100	100

Note on Table 5: Relative CIGS volume (%) = (thickness / maximum thickness) × 100, with maximum thickness = 4 µm. Retained efficiency (%) = (η at the considered thickness / η at 4 µm) × 100, calculated separately for the with- and without-MgF_2 configurations from the η values shown in Figure 6.

At very low thicknesses, however, the literature on ultra-thin CIGS reports substantially lower efficiencies than those obtained here at comparable thickness (22.17%/19.69% at 1 µm with/without MgF_2 in the present study) [16, 31]. This gap suggests that the present model may underestimate some of the additional losses experimentally associated with ultra-thin CIGS absorbers. Because the electronic and defect parameters are intentionally kept unchanged during the thickness sweep, effects such as thickness-dependent microstructural degradation, enhanced interface sensitivity, or changes in defect density are not captured here, consistent with the correlated increase in R_s described in Section 3.3 [21]. Significantly reducing thickness below 1 µm would therefore only be reasonable in combination with dedicated passivation strategies (back-surface field, double-layer antireflection stack [29], bandgap grading [32]), not modeled in this work.

The MgF_2 layer, being purely optical and consuming neither indium nor gallium, thus constitutes a particularly attractive lever to offset part of the efficiency loss associated with absorber thinning. Figure 6 shows that a cell with only 1 µm of CIGS fitted with MgF_2 reaches 22.17%, exceeding the 21.93% obtained with a four-times-thicker absorber without MgF_2, for a quarter of the CIGS volume; likewise, a 0.5 µm cell with MgF_2 (20.40%) exceeds a 1 µm cell without MgF_2 (19.69%). Combining a thinned absorber with a low-cost antireflection coating can therefore match, or even exceed, the efficiency of a substantially thicker cell lacking such a coating.

Within the investigated range, 2–3 µm combined with MgF_2 therefore provides the most favorable performance/material-use trade-off, retaining 96–98% of the maximum simulated efficiency while requiring only 50–75% of the CIGS volume used at 4 µm. Reducing thickness below 1 µm remains conceivable for the material saving it provides, but likely exposes the device to additional losses not captured here, barring the use of complementary passivation strategies. This trade-off, derived from the analysis of the full interval rather than from the single 4 µm point, would benefit from experimental confirmation and from refinement through an explicit process-cost model incorporating, beyond the active material, deposition time and the cost of the glass substrate and TCO, largely independent of absorber thickness.

3.7. Summary

Table 6 summarizes the trends observed over the studied thickness range (0.5 to 4 µm).

Table 6. *Overall contribution of CIGS thickness and the MgF_2 antireflection coating.*

Parameter	Effect of CIGS thickness	Effect of the MgF_2 layer
J_{sc}	Monotonic increase (+11.3%)	Nearly constant relative gain (~12.2%)
V_{oc}	Moderate, logarithmic increase (+6.0%)	Marginal gain (~2–3 mV)
FF	Monotonic increase (82.2% → 84.3%)	Not significant
R_s (effective)	Monotonic decrease (≈−12%)	Lower (apparent effect, linked to the J_{sc} shift)
R_{sh} (effective)	Strong increase (×3.5 approx.)	Lower with MgF_2 (apparent effect)
η	Continuous increase up to 4 µm, saturation beyond 3 µm	Nearly constant relative gain of about 12.6%, inherited from J_{sc}

4. Discussion, Limitations and Outlook

The trends obtained in this work are consistent with the broader landscape of the literature on the optimization of non-toxic-buffer CIGS cells: the continuous increase in efficiency with thickness, the progressive saturation of J_{sc} beyond 2.5–3 µm, and the nearly constant relative gain provided by MgF_2 are in line with the order of magnitude reported for related architectures [17, 33, 34], while the simulated efficiencies (18.1%–24.7% depending on configuration and thickness) remain within the expected performance range for this type of structure, below the absolute records achieved on fully optimized cells co-doped with heavy alkali elements [8, 9], themselves representative of the current state of the art in the CIGS field [2].

The explicit integration of the parasitic resistances R_s and R_{sh} into the interpretation of the electrical results is a complement rarely developed in parametric studies focused solely on the J_{sc}/V_{oc}/FF triplet. By quantitatively connecting the effective decrease in R_s and increase in R_{sh} to the continuous improvement of the fill factor with thickness, this analysis goes beyond a purely optical-absorption reading, in line with earlier work that highlighted the diagnostic value of these two resistances for CIGS/In_2S_3 cells [18].

This study nonetheless has certain limitations, inherent to any TCAD simulation approach. The results rest on a set of material parameters (Table 2) that were kept constant throughout the thickness sweep so as to isolate the geometric effect of the absorber. This controlled comparison does not reproduce possible variations in microstructure, defect density, or crystalline quality that may experimentally accompany a reduction in CIGS thickness. The results should accordingly be interpreted as trends intrinsic to the model considered, whose full quantitative validation will require comparison with experimental devices of comparable architecture. The interface-defect model likewise remains simplified, using a single Dit value without a detailed energy distribution. Finally, as discussed in Section 3.3, the apparent dependence of R_s and R_{sh} on the presence of MgF_2 is more plausibly associated with the sensitivity of the slope-based extraction procedure to the MgF_2-induced shift of the J–V characteristic than with a direct physical modification of the device resistive elements. Accordingly, these conclusions apply strictly to absorber-thickness variation under otherwise constant material quality, doping, and interface-defect density; extending them to devices where thickness and material quality vary jointly would require these parameter variations to be incorporated explicitly.

Future work should prioritize experimental validation of the simulated thickness trends, joint optimization of absorber thickness and doping, and extension to thickness/bandgap-grading strategies in order to determine how robust the identified performance/material-use trade-off remains under more realistic device conditions.

5. Conclusion

This study numerically examined, using the Silvaco ATLAS simulator, the effect of CIGS absorber thickness (0.5 to 4 µm) on the performance of an In_2S_3-buffered thin-film solar cell, building on an earlier doping-optimization study conducted on the same layer stack. Two otherwise identical structures, one including a MgF_2 front-surface antireflection coating and the other without, were compared at fixed optimal doping ($N_A = 3\times10^{16}$ cm^{-3}), so as to isolate the specific contribution of absorber thickness from that of the antireflection coating.

The MgF_2 coating provides a nearly thickness-independent relative efficiency gain of about 12.6% over the investigated 0.5–4 µm range, arising almost entirely from the increase in J_{sc}, with only minor changes in V_{oc} and FF, indicating that this optical benefit acts largely independently of the separate, thickness-driven improvement in performance. This decoupling has a direct practical consequence: a 1 µm CIGS absorber combined with MgF_2 (η = 22.17%) already outperforms a 4 µm absorber without MgF_2 (η = 21.93%), using only a quarter of the active-material volume, demonstrating that improved front-surface optical management can compensate for a substantial reduction in absorber thickness. More broadly, CIGS thickness is found to primarily drive short-circuit current and, to a lesser extent, open-circuit voltage, with efficiency increasing continuously up to 4 µm and no optimum or degradation observed over the studied range.

The effective R_s and R_{sh} values extracted from the simulated J–V curves provide complementary diagnostic information on the evolution of the fill factor with absorber thickness. Their effective decrease and increase, respectively, track the improvement of FF and are qualitatively consistent with published experimental trends in CIGS-based thin-film cells. The apparent gaps between the with- and without-MgF_2 configurations most likely reflect the sensitivity of the slope-based extraction to the MgF_2-induced shift of the J–V characteristic rather than a genuine change in the physical resistive elements of the device.

The marginal-gain analysis over the full swept thickness interval (Section 3.6), rather than the single value reached at 4 µm, indicates that a thickness of about 2–3 µm combined with the MgF_2 layer constitutes the best performance/material-use trade-off identified by this study: it preserves 96–98% of the maximum simulated efficiency for only 50–75% of the CIGS volume engaged at 4 µm, with the 4 µm configuration remaining nonetheless preferable whenever absolute efficiency takes precedence over material economy. This trade-off holds under the constant-material-quality scope discussed in Section 4; confronting it with experimental devices spanning this thickness range, and extending the approach to a joint thickness/doping or thickness/bandgap-grading optimization, are natural next steps. Absorber-thickness optimization and front-surface optical management thus emerge as two complementary design levers for CIGS/In_2S_3 solar cells, with the joint

analysis of R_s and R_{sh} providing a useful diagnostic framework for interpreting the associated evolution of the fill factor.

Abbreviations

ATLAS	Silvaco Semiconductor Device Simulation Module
AM1.5G	Terrestrial Reference Solar Spectrum (Air Mass 1.5 Global)
CIGS	$Cu(In,Ga)Se_2$, Copper Indium Gallium Diselenide (Absorber)
FF	Fill Factor
In_2S_3	Indium Sulfide (Buffer Layer)
MgF_2	Magnesium Fluoride (Antireflection Coating)
Mo	Molybdenum (Back Contact)
SRH	Shockley-Read-Hall (Recombination Model)
TCAD	Technology Computer-Aided Design
TCO	Transparent Conductive Oxide
AZO	Aluminum-doped Zinc Oxide (ZnO:Al)

Author Contributions

Papa Lat Tabara Sow: Conceptualization, Formal Analysis, Investigation, Methodology, Writing – original draft

Cheick Tidiane Goudiaby: Conceptualization, Formal Analysis, Investigation, Methodology, Writing – original draft

Alioune Ngom: Formal Analysis, Investigation, Writing– original draft

Jacques Joachim Faye: Formal Analysis, Investigation, Methodology

Ahmed Mohamed-Yahya: Formal Analysis, Validation, Writing – review & editing

Mamadou Lamine Samb: Conceptualization, Methodology, Supervision, Validation, Writing – review & editing

Conflicts of Interest

The authors declare no conflicts of interest.

Appendix

Symbols

d	CIGS Absorber Thickness (μm)
D_{it}	Interface Defect Density (cm^{-2} eV^{-1})
E_g	Optical Bandgap Energy (eV)
J_{sc}	Short-Circuit Current Density (mA cm^{-2})
N_A	Acceptor Concentration (cm^{-3})
P_{in}	Incident Power Density (mW cm^{-2})
R_s	Effective Series Resistance ($\Omega \cdot cm^2$)
R_{sh}	Effective Shunt Resistance ($\Omega \cdot cm^2$)
V_{oc}	Open-Circuit Voltage (V)
η	Conversion Efficiency (%)

References

[1] A. Luque, S. Hegedus (Eds.). Handbook of Photovoltaic Science and Engineering. 2nd ed. Chichester, UK: Wiley; 2011. https://doi.org/10.1002/9780470974704

[2] M. Powalla, S. Paetel, D. Hariskos, R. Wuerz, F. Kessler, P. Lechner, W. Wischmann, T. M. Friedlmeier. Advances in cost-efficient thin-film photovoltaics based on $Cu(In,Ga)Se_2$. Engineering. 2017, 3(4), 445–451. https://doi.org/10.1016/J.ENG.2017.04.015

[3] D. Hariskos, S. Spiering, M. Powalla. Buffer layers in $Cu(In,Ga)Se_2$ solar cells and modules. Thin Solid Films. 2005, 480–481, 99–109. https://doi.org/10.1016/j.tsf.2004.11.118

[4] W. Shafarman, S. Siebentritt, L. Stolt. $Cu(In,Ga)Se_2$ solar cells. In: Handbook of Photovoltaic Science and Engineering. 2nd ed. Chichester, UK: Wiley; 2011, 546–599. https://doi.org/10.1002/9780470974704.ch13

[5] S. M. Sze, K. K. Ng. Physics of Semiconductor Devices. 3rd ed. Hoboken, NJ, USA: Wiley-Interscience; 2007. https://doi.org/10.1002/0470068329

[6] I. Repins, M. A. Contreras, B. Egaas, C. DeHart, J. Scharf, C. L. Perkins, B. To, R. Noufi. 19.9%-efficient ZnO/CdS/$CuInGaSe_2$ solar cell with 81.2% fill factor. Progress in Photovoltaics: Research and Applications. 2008, 16, 235–239. https://doi.org/10.1002/pip.822

[7] P. Jackson, D. Hariskos, E. Lotter, S. Paetel, R. Wuerz, R. Menner, W. Wischmann, M. Powalla. New world record efficiency for $Cu(In,Ga)Se_2$ thin-film solar cells beyond 20%. Progress in Photovoltaics: Research and Applications. 2011, 19, 894–897. https://doi.org/10.1002/pip.1078

[8] P. Jackson, R. Wuerz, D. Hariskos, E. Lotter, W. Witte, M. Powalla. Effects of heavy alkali elements in $Cu(In,Ga)Se_2$ solar cells with efficiencies up to 22.6%. Physica Status Solidi (RRL). 2016, 10(8), 583–586. https://doi.org/10.1002/pssr.201600199

[9] M. Nakamura, K. Yamaguchi, Y. Kimoto, Y. Yasaki, T. Kato, H. Sugimoto. Cd-Free $Cu(In, Ga)(Se, S)_2$ Thin-Film Solar Cell with Record Efficiency of 23.35%. IEEE Journal of Photovoltaics. 2019, 9(6), 1863–1867. https://doi.org/10.1109/JPHOTOV.2019.2937218

[10] M. Boubakeur, A. Aissat, M. Ben Arbia, H. Maaref, J. P. Vilcot. Enhancement of the efficiency of ultra-thin CIGS/Si structure for solar cell applications. Superlattices and Microstructures. 2020, 138, 106377. https://doi.org/10.1016/j.spmi.2019.106377

[11] R. Saez-Araoz, J. Krammer, S. Harndt, T. Kohler, M. Kruger, P. Pistor et al. ILGAR In_2S_3 buffer layers for Cd-free $Cu(In, Ga)(S, Se)_2$ solar cells with certified efficiencies above 16%. Progress in Photovoltaics: Research and Applications. 2012, 20, 855–861. https://doi.org/10.1002/pip.2268

[12] Silvaco Inc. ATLAS User's Manual: Device Simulation Software. Santa Clara, CA, USA: Silvaco International; 2016.

[13] W. Shockley, W. T. Read. Statistics of the Recombinations of Holes and Electrons. Physical Review. 1952, 87(5), 835–842. https://doi.org/10.1103/PhysRev.87.835

[14] T. Minemoto, T. Matsui, H. Takakura, Y. Hamakawa, T. Negami, Y. Hashimoto, T. Uenoyama, M. Kitagawa. Theoretical analysis of the effect of conduction band offset of window/CIS layers on performance of CIS solar cells using device simulation. Solar Energy Materials and Solar Cells. 2001, 67(1–4), 83–88. https://doi.org/10.1016/S0927-0248(00)00266-X

[15] N. Khoshsirat, N. A. Md Yunus. Copper-Indium-Gallium-diSelenide (CIGS) Nanocrystalline Bulk Semiconductor as the Absorber Layer and Its Current Technological Trend and Optimization. In: Nanoelectronics and Materials Development. InTech; 2016, 41–58. https://doi.org/10.5772/64166

[16] H. Heriche, Z. Rouabah, N. Bouarissa. New ultra thin CIGS structure solar cells using SCAPS simulation program. International Journal of Hydrogen Energy. 2017, 42(15), 9524–9532. https://doi.org/10.1016/j.ijhydene.2017.02.099

[17] N. Khoshsirat, N. A. Md Yunus. Numerical Analysis of In_2S_3 Layer Thickness, Band Gap and Doping Density for Effective Performance of a CIGS Solar Cell Using SCAPS. Journal of Electronic Materials. 2016, 45(11), 5721–5727. https://doi.org/10.1007/s11664-016-4744-6

[18] Y. Gning, M. Biagui, M. Tour é, A. Tour é, M. L. Samb. Donor-Doping Optimization of In_2S_3 Buffer Layers in CIGS Solar Cells: A TCAD Diagnostic of Transport-Recombination-Leakage Competition via Rs and Rsh. Journal of Materials Science and Chemical Engineering. 2026, 14(4), 1–19. https://doi.org/10.4236/msce.2026.144001

[19] S. S. Hegedus, W. N. Shafarman. Thin-film solar cells: device measurements and analysis. Progress in Photovoltaics: Research and Applications. 2004, 12(2–3), 155–176. https://doi.org/10.1002/pip.518

[20] R. Carron, E. Avancini, T. Feurer, B. Bissig, P. A. Losio, R. Figi et al. Refractive indices of layers and optical simulations of $Cu(In,Ga)Se_2$ solar cells. Science and Technology of Advanced Materials. 2018, 19(1), 396–410. https://doi.org/10.1080/14686996.2018.1458579

[21] E. Maria, A. Saha, M. R. Khan, M. A. Zubair, M. Z. Baten, R. N. Sajjad. Carrier transport and performance limit of semi-transparent photovoltaics: $CuIn_{1-x}Ga_xSe_2$ as a case study. Journal of Applied Physics. 2021, 130(17), 173106. https://doi.org/10.1063/5.0063930

[22] T. D. Lee, A. U. Ebong. A review of thin film solar cell technologies and challenges. Renewable and Sustainable Energy Reviews. 2017, 70, 1286–1297. https://doi.org/10.1016/j.rser.2016.12.028

[23] Y. Wei, Z. Ma, X. Zhao, J. Yin, Y. Wu, L. Zhang, M. Zhao. Improving the performance of $Cu_2ZnSn(S, Se)_4$ thin film solar cells by SCAPS simulation. Materials Science and Engineering: B. 2024, 303, 117296. https://doi.org/10.1016/j.mseb.2024.117296

[24] S. Upadhyay, D. Singh. Effect of Series and Shunt Resistance on the Performance of Kesterite Solar Cells. International Journal of Scientific Research in Modern Science and Technology. 2023, 2(8), 38–45.

[25] M. F. Rahman, M. Chowdhury, L. Marasamy, M. K. A. Mohammed, M. D. Haque, S. R. Al Ahmed, A. Irfan, A. R. Chaudhry, S. Goumri-Said. Improving the efficiency of a CIGS solar cell to above 31% with Sb_2S_3 as a new BSF: a numerical simulation approach by SCAPS-1D. RSC Advances. 2024, 14(3), 1924–1938. https://doi.org/10.1039/D3RA07893K

[26] N. Rezaei, O. Isabella, Z. Vroon, M. Zeman. Optical optimization of a multi-layer wideband anti-reflection coating using porous MgF_2 for sub-micron-thick CIGS solar cells. Solar Energy. 2019, 177, 59–67. https://doi.org/10.1016/j.solener.2018.11.015

[27] G. Rajan, S. Karki, R. W. Collins, N. J. Podraza, S. Marsillac. Real-Time Optimization of Anti-Reflective Coatings for CIGS Solar Cells. Materials. 2020, 13(19), 4259. https://doi.org/10.3390/ma13194259

[28] R. Serhane et al. Effect of Anti-Reflective Coating on CIGS Solar Cells Performance. IEEE Conference Publication; 2021.

[29] F. Ahmad, B. J. Civiletti, P. B. Monk, A. Lakhtakia. Double-layer antireflection coatings for CIGS thin-film solar cells. Proceedings of SPIE. 2023, 12477, 124770E. https://doi.org/10.1117/12.2645881

[30] A. Ravilla, E. Gullickson, A. Tomes, I. Celik. Economic and environmental sustainability of copper indium gallium selenide (CIGS) solar panels recycling. Science of the Total Environment. 2024, 951, 175670. https://doi.org/10.1016/j.scitotenv.2024.175670

[31] K. Ramanathan, J. Keane, R. Noufi. Properties of High-Efficiency CIGS Thin-Film Solar Cells. In: Proceedings of the 31st IEEE Photovoltaic Specialists Conference; 2005; Lake Buena Vista, FL, USA; pp. 195–198. NREL/CP-520-37404. https://doi.org/10.1109/PVSC.2005.1488103

[32] F. Ahmad, T. H. Anderson, P. B. Monk, A. Lakhtakia. Efficiency enhancement of ultrathin CIGS solar cells by optimal bandgap grading. Applied Optics. 2019, 58(22), 6067–6078. https://doi.org/10.1364/AO.58.006067

[33] R. N. Mohottige, S. P. Kalawila Vithanage. Numerical simulation of a new device architecture for CIGS-based thin-film solar cells using 1D-SCAPS simulator. Journal of Photochemistry and Photobiology A: Chemistry. 2021, 407, 113079. https://doi.org/10.1016/j.jphotochem.2020.113079

[34] A. Kumar, S. M. Giripunje, A. K. Patel, S. Gohri. Designing and simulating of new highly efficient ultra-thin CIGS solar cell device structure: Plan to minimize cost per watt price. Journal of Physics and Chemistry of Solids. 2024, 193, 112194. https://doi.org/10.1016/j.jpcs.2024.112194